Author Manuscript

Author Manuscript

Author Manuscript

Author Manuscript

HHS Public Access

Author manuscript

Sci Transl Med. Author manuscript; available in PMC 2016 December 29.

Published in final edited form as:

Sci Transl Med. 2016 June 29; 8(345): 345ra87. doi:10.1126/scitranslmed.aaf7374.

P-selectin is a nanotherapeutic delivery target in the tumor microenvironment

Yosi Shamay[1], **Moshe Elkabets**[2,3], **Hongyan Li**[4], **Janki Shah**[1], **Samuel Brook**[2], **Feng Wang**[4,5], **Keren Adler**[1,6], **Emily Baut**[1,7], **Maurizio Scaltriti**[2,8], **Prakrit V. Jena**[1], **Eric E. Gardner**[1,9], **John T. Poirier**[1,7,10], **Charles M. Rudin**[1,7,10], **José Baselga**[2,10], **Adriana Haimovitz-Friedman**[4], and **Daniel A. Heller**[1,7,*]

[1]Molecular Pharmacology Program, Memorial Sloan Kettering Cancer Center, New York, NY 10065, USA

[2]Human Oncology and Pathogenesis Program, Memorial Sloan Kettering Cancer Center, New York, NY 10065, USA

[3]The Shraga Segal Department of Microbiology, Immunology and Genetics, Faculty of Health Sciences, Ben-Gurion University of the Negev, Beer-Sheva 84105, Israel

[4]Department of Radiation Oncology, Memorial Sloan Kettering Cancer Center, New York, NY 10065, USA

[5]Department of Oncology, Albert Einstein Cancer Center, Albert Einstein College of Medicine, New York, NY 10461, USA

[6]Brandeis University, Waltham, MA 02453, USA

[7]Weill Cornell Medical College, New York, NY 10065, USA

[*]Corresponding author. hellerd@mskcc.org.

SUPPLEMENTARY MATERIALS

www.sciencetranslationalmedicine.org/cgi/content/full/8/345/345ra87/DC1

Fig. S1. Isotype controls and major genomic alterations.
Fig. S2. Nanoparticle characterization.
Fig. S3. In vitro and in vivo nanoparticle targeting studies.
Fig. S4. P-selectin and CD31 expression in irradiated and contralateral unirradiated tumors.
Fig. S5. Effect of ionizing radiation on P-selectin and nanoparticle localization.
Fig. S6. In vivo bioluminescence of metastatic models 7 days after treatments.
Fig. S7. B16F10 melanoma model assessments.
Fig. S8. Cytokine profile in the serum of healthy mice injected with FiPAX nanoparticles.
Fig. S9. P-selectin–targeted nanoparticle delivery of a MEK/ERK inhibitor.
Fig. S10. Kinetics of pERK inhibition in an HCT116 xenograft model.
Table S1. Nanoparticle sizes in nanometers, as measured by DLS.
Table S2. Complete blood count conducted 24 hours after intravenous administration of nanoparticles in healthy mice.

Author contributions: Y.S. and DAH. conceived the project and designed experiments. Y.S. and M.E. analyzed TCGA data and designed and conducted the MEK-related experiments. Y.S. and J.S. performed the in vivo experiments, electron microscopy, and tissue staining. Y.S. developed the tumor spheroids. H.L. performed all radiation-related experiments. S.B. performed in vitro experiments with MEK inhibitor. J.T.P. and C.M.R. developed PDX models of SCLC. K.A. optimized particle synthesis and Transwell assays. P.VJ. analyzed data. M.S., J.B., C.M.R., A.H.-F., and D.A.H. supervised the research. Y.S., M.E., M.S., and D.A.H. wrote the manuscript. E.B. prepared FiPAX nanoparticles. E.E.G. generated LX33 lung PDX xenografts. F.W. performed in vitro radiation treatments.

Competing interests: J.B. has consulted for Novartis Pharmaceuticals and serves on the board of Infinity Pharmaceuticals. C.M.R. has been a paid consultant regarding oncology drug development with Bristol-Myers Squibb, Celgene, Medivation, and Novartis. Y.S. and D.A.H. have a pending patent for the targeted nanoparticle technology.

Author Manuscript Author Manuscript Author Manuscript Author Manuscript

[8]Department of Pathology, Memorial Sloan Kettering Cancer Center, New York, NY 10065, USA

[9]Pharmacology Graduate Training Program, Johns Hopkins University, Baltimore, MD 21287, USA

[10]Department of Medicine, Memorial Sloan Kettering Cancer Center, New York, NY 10065, USA

Abstract

Disseminated tumors are poorly accessible to nanoscale drug delivery systems because of the vascular barrier, which attenuates extravasation at the tumor site. We investigated P-selectin, a molecule expressed on activated vasculature that facilitates metastasis by arresting tumor cells at the endothelium, for its potential to target metastases by arresting nanomedicines at the tumor endothelium. We found that P-selectin is expressed on cancer cells in many human tumors. To develop a targeted drug delivery platform, we used a fucosylated polysaccharide with nanomolar affinity to P-selectin. The nanoparticles targeted the tumor microenvironment to localize chemotherapeutics and a targeted MEK (mitogen-activated protein kinase kinase) inhibitor at tumor sites in both primary and metastatic models, resulting in superior antitumor efficacy. In tumors devoid of P-selectin, we found that ionizing radiation guided the nanoparticles to the disease site by inducing P-selectin expression. Radiation concomitantly produced an abscopal-like phenomenon wherein P-selectin appeared in unirradiated tumor vasculature, suggesting a potential strategy to target disparate drug classes to almost any tumor.

INTRODUCTION

The clinical potential of nanomedicines has not yet been fulfilled (1, 2), in part because of the endothelial barrier, which limits extravasation of nanoparticles at the sites of solid tumors (3–5). Passive targeting mechanisms, such as the enhanced permeability and retention (EPR) effect (6), show some promise, but they have not yet demonstrated notable benefit in disseminated tumors (7) or in patients (4). Tumor vasculature, which is composed of smooth muscle cells, pericytes, extracellular matrix, and endothelial cells (ECs), is necessary for the growth and support of tumors. The EC component of tumor neovasculature is a promising target for antitumor therapy because of its genetic stability, exposure to the circulation, and direct access from the intravascular space (8). Nanoparticle drug carriers targeting the neovasculature are currently under clinical development (9); however, targeted delivery of therapeutic agents to micrometastases or tumors lacking neovasculature remains a persistent challenge (10).

P-selectin, an inflammatory cell adhesion molecule responsible for leukocyte recruitment and platelet binding (11–14), is expressed constitutively in ECs, where it is stored in intracellular granules known as Weibel-Palade bodies. Upon endothelial activation with endogenous cytokines (15) or exogenous stimuli such as ionizing radiation (16–19), P-selectin translocates to the cell membrane and into the lumen of blood vessels. Elevated P-selectin expression has been found in the vasculature of human lung (20), breast (21), and kidney cancers (22). Moreover, P-selectin facilitates the process of metastasis by promoting the adhesion of circulating cancer cells to activated platelets and endothelium in distant organs (12, 13). These associations with tumors and micrometastases, as well its induction

Author Manuscript Author Manuscript Author Manuscript Author Manuscript

with radiation, suggest P-selectin as a possible target for cancer drug delivery and radiation-guided drug delivery (23).

We investigated P-selectin as a target for localized drug delivery to tumor sites, including metastases. We found that many human tumors express P-selectin on tumor cells and in tumor vasculature, whereas normal tissues exhibit little expression. To target drugs to P-selectin–expressing tumors, we synthesized a nanoparticle carrier for chemotherapeutic drugs and targeted therapeutics using the algae-derived polysaccharide fucoidan, which exhibits nanomolar affinity for P-selectin (24–29). These fucoidan-based nanoparticles targeted activated endothelium, demonstrated penetration of endothelial barriers in vitro, and exhibited a therapeutic advantage over untargeted chemotherapeutic drugs or passively targeted nanoparticles in P-selectin–expressing tumors and metastases in vivo. The encapsulation of MEK162, a reversible MEK [mitogen-activated protein kinase (MAPK) kinase] inhibitor, conferred a therapeutic benefit in P-selectin–expressing tumors, including an increase in phosphorylated extracellular signal–regulated kinase (pERK) inhibition and tumor cell apoptosis as compared to the free drug without suppression of pERK in the skin, suggesting the potential for the amelioration of a major MEK inhibitor toxicity and increased therapeutic index. Upon exposure to ionizing radiation, which induced expression of P-selectin, nanoparticles localized in the irradiated tumor site and conferred substantial inhibition in tumors that did not spontaneously express the target. In addition, in mice bearing bilateral tumors, delivery of radiation to one tumor resulted in nanoparticle localization in the contralateral, unirradiated tumor, an effect reminiscent of the abscopal effect, wherein localized radiotherapy causes distant tumors to respond.

RESULTS

Expression of P-selectin in human cancers

To determine the prevalence of P-selectin protein expression in cancer tissues, we assessed 420 clinical samples by immunohistochemistry (IHC). We found that P-selectin is expressed within multiple tumor types, including lung (19%), ovarian (68%), lymphoma (78%), and breast (49%) (Fig. 1, A and B, and fig. S1A). As expected, we found abundant expression of P-selectin in the vasculature surrounding the tumor cells but not in adjacent normal tissue. In a subset of cancers, P-selectin expression was also observed on tumor cells and/or stroma (Fig. 1A). To corroborate this finding, we interrogated The Cancer Genome Atlas (TCGA) for P-selectin (*SELP*) staining, RNA expression, and common *SELP* genomic alterations in tumor tissues. The TCGA database revealed elevated RNA expression in multiple tumors (Fig. 1C) and amplifications in several human cancers such as melanoma (15.5%), liver cancer (15%), bladder urothelial carcinoma (13.4%), and lung adenocarcinoma (12.2%) (fig. S1B).

A P-selectin–targeted nanoparticle drug carrier

To design a P-selectin–targeted drug delivery system, we prepared nanoparticles composed of fucoidan (Fi) to encapsulate three different drugs. Fucoidan-encapsulated paclitaxel (PAX) nanoparticles (FiPAX) were synthesized by coencapsulating paclitaxel and a near-infrared (NIR) fluorophore (IR-783), to facilitate imaging, via nanoprecipitation (Fig. 1D,

Author Manuscript Author Manuscript Author Manuscript Author Manuscript

top). A specific inhibitor of MEK, MEK162, was similarly encapsulated in fucoidan nanoparticles (FiMEK) by the same method. Fucoidan-encapsulated doxorubicin (DOX) nanoparticles (FiDOX) were synthesized via layer-by-layer assembly of a cationic doxorubicin-polymer conjugate [DOX-PEG-DOX (DPD)] and the anionic fucoidan (Fig. 1D, bottom). The DPD conjugate was synthesized with pH-cleavable hydrazone linkages to promote drug release within the acidic tumor microenvironment or within acidic organelles upon endocytosis. The FiPAX, FiMEK, and FiDOX nanoparticles measured 105 ± 4.2, 85 ± 3.6, and 150 ± 8.1 nm in diameter, respectively, and they exhibited about −55 mV ζ potential (surface charge) (fig. S2, A and B). Electron microscopy showed relatively uniform spherical morphologies (fig. S2C). The nanoparticles exhibited good serum stability over 5 days and pH-dependent drug release rates (fig. S2, D to G), and they could be reconstituted after lyophilization.

Nanoparticle binding to P-selectin

To assess the targeting selectivity to P-selectin, we synthesized a drug-loaded nanoparticle lacking the fucoidan component, as a control for targeting studies. Dextran sulfate–based nanoparticles with comparable physical properties to those of FiPAX nanoparticles were assembled by the same methods as used above (Fig. 1D, fig. S2, and table S1). We assessed the binding of fucoidan-based (FiPAX) and control (DexPAX) nanoparticles to immobilized human recombinant P-selectin, L-selectin, E-selectin, and bovine serum albumin (BSA). The experiment demonstrated selective dose-dependent binding of fucoidan-based nanoparticles to P-selectin and almost no binding to L-sdectin, E-sekctin, or BSA (Fig. 1E).

To assess the binding of fucoidan-based nanoparticles to P-selectin–expressing tissues, we used a murine cell line, SK-136 (30), which formed multicellular tumor spheroids and constitutively expresses P-selectin (Fig. 2A). Penetration of the nanoparticles into the tumor spheres was quantified by fluorescence microscopy. Upon incubation with the spheroids for 20 min, the FiPAX nanoparticle fluorescence was five times greater, as compared to the DexPAX nanoparticle control (Fig. 2, B and C; $P = 0.0042$).

The binding of nanoparticles to a monolayer of ECs was measured under simulated inflammatory conditions to induce P-selectin expression (31). Upon activation with tumor necrosis factor–α (TNFα) or ionizing radiation (6 Gy), FiPAX nanoparticles bound to EA.hy926 cells, as evinced by a large increase in fluorescence signal from the cells (Fig. 2D). All controls, including the TNFα-negative condition and DexPAX nanoparticles, exhibited virtually no signal. Cells treated with short hairpin RNA to knock down P-selectin expression exhibited a marked decrease in particle binding, further validating the P-selectin–mediated targeting properties of the fucoidan-based nanoparticles (fig. S3, A and B). The nanoparticle-mediated cytotoxicity was evaluated under similar conditions of endothelial activation (Fig. 2E). The median inhibitory concentration (IC_{50}) of FiPAX was much lower, as compared to DexPAX, further confirming the selectivity of the fucoidan-based nanoparticles to P-selectin (Fig. 2E).

Author Manuscript Author Manuscript Author Manuscript Author Manuscript

In vitro assessment of nanoparticle penetration through endothelial barriers

The ability of fucoidan nanoparticles to penetrate through activated endothelium and into tumor tissue was assessed using a modified Transwell assay. Murine brain endothelial (bEnd.3) cells (32, 33) were grown on the membrane of the upper chambers. Tumor spheroids derived from P-selectin–expressing SK-136 cells (fig. S3C) were grown in the bottom chambers (Fig. 2F). The penetration of the nanoparticles through the bEnd.3 monolayers was measured under inflammatory conditions using TNFα activation, which induces P-selectin expression (31). One hour after the addition of FiPAX nanoparticles to the top chambers, the quantity of FiPAX nanoparticles recovered from the bottom chamber increased by about 30% (Fig. 2G) in the presence of TNFα, and recovery of DexPAX nanoparticles increased by 15% relative to nonactivated conditions. Penetration of the nanoparticles into the tumor spheres in the bottom well of the assay plates was quantified by fluorescence microscopy. The FiPAX nanoparticles exhibited a three times higher signal in the tumor spheroids in the presence of TNFα, as well as greater penetration into the spheres, as compared to the controls (fig. S3, D to F). These observations suggest that endothelial activation mediated increased transport of P-selectin–targeted nanoparticles across the endothelial barrier, which resulted in greater penetration into solid tumor tissue. Encouraged by these findings, we explored the penetration and antitumor activity of FiPAX in P-selectin–expressing tumors in vivo.

In vivo targeting and antitumor efficacy mediated by P-selectin

To determine the efficacy of P-selectin targeting compared to passive mechanisms of drug delivery in vivo, the patient-derived xenograft (PDX) model of SCLC, JHU-LX33 (34), was used. The xenograft expressed P-selectin in the tumor endothelium and moderately in the cancer cells, as observed by IHC (Fig. 3A, top). When tumors reached 70 mm^3, mice were randomized into four treatment arms: vehicle [phosphate-buffered saline (PBS)], FiPAX, DexPAX, and free paclitaxel (PAX). At 24 hours after injection, the average fluorescence intensity of FiPAX nanoparticles in the tumor, as measured by in vivo fluorescence imaging, reached 2.5-fold higher than that of passively targeted DexPAX nanoparticles. The signal difference increased to 4.1-fold at 72 hours after injection (Fig. 3A, bottom, and fig. S3, G and H). The biodistribution, measured by fluorescence, showed substantial selective accumulation of FiPAX nanoparticles in the tumor over healthy organs, yielding a signal 3.6-fold higher in the tumor than the combined signal from all organs (fig. S3H). The same calculation made for DexPAX nanoparticles was only 1.3-fold, suggesting superior tumor targeting mediated by P-selectin with an improvement of 2.8-fold over passive targeting mechanisms. Improved tumor inhibition was observed upon administration of a single dose of FiPAX nanoparticles, as compared to free paclitaxel or DexPAX nanoparticles, all administered with equal drug concentrations (Fig. 3B).

Radiation-guided drug delivery mediated by P-selectin

To study the effect of tumor irradiation on P-selectin targeting in vivo, we used the Lewis lung carcinoma model, a mouse tumor model that does not spontaneously express P-selectin. We inoculated immunocompetent, hairless SKH-1 mice in both flanks with Lewis lung carcinoma (3LL) cells. The resulting tumor did not endogenously express P-selectin, as

Author Manuscript Author Manuscript Author Manuscript Author Manuscript

demonstrated by tissue staining (Fig. 3C). We irradiated the right flank tumor of each mouse with an x-ray dose of 6 Gy, and the left flank tumor was left unirradiated. The appearance of P-selectin in the irradiated tumor was apparent by 4 hours, and the amount increased substantially by 24 hours (Fig. 3D). Costaining for P-selectin and CD31 shows that P-selectin was localized mainly to the endothelium after radiation treatment (fig. S4). P-selectin staining was also seen around vessels in smaller, scattered punctate patches, suggesting the presence of activated platelets (14).

We also detected the presence of P-selectin in the unirradiated left flank tumors 24 hours after irradiation of the right flank tumors, suggesting immune activation of distant sites—a phenomenon reminiscent of the abscopal effect (35). This phenomenon was accompanied by a substantial increase of soluble P-selectin (sP-selectin) in the blood (fig. S5A).

We studied whether radiation could selectively guide P-selectin–targeted drug carrier nanoparticles to the tumor site and result in a therapeutic benefit. The right flank tumors of the bilateral 3LL xeno-grafted mice were irradiated with 6 Gy before injecting nanoparticles intravenously 4 hours later. To distinguish the effects of radiation-induced P-selectin targeting from EPR-mediated accumulation or the targeting of non–radiation-induced P-selectin, we included experimental arms using DexPAX nanoparticles and nonirradiated mouse controls. At 24 hours after treatment, the fluorescence signal in the FiPAX-treated tumors was 3.8-fold higher in the irradiated tumors over nonirradiated tumors, but there was no difference in the DexPAX-treated mice (Fig. 3E and fig. S5B). Growth was inhibited in tumors receiving both radiation and FiPAX nanoparticles, resulting in complete and durable tumor regression (Fig. 3F). In mice treated with irradiation and FiPAX nanoparticles, significant ($P = 0.0031$) tumor growth inhibition was observed also in the unirradiated left flank tumors (Fig. 3F). Immunofluorescence microscopy of tumor slices 24 hours after treatment revealed substantial apoptosis in both tumor and ECs in the irradiated tumors treated with FiPAX, as measured by TUNEL (terminal deoxynucleotidyl transferase–mediated deoxyuridine triphosphate nick end labeling) staining (fig. S5C).

P-selectin-mediated antitumor efficacy in a metastatic model

We assessed the antitumor efficacy of P-selectin–targeted drug carrier nanoparticles against two aggressive experimental metastasis models of melanoma and breast cancer (36, 37). The intravenous injection of 10^5 firefly luciferase–expressing B16F10 melanoma or firefly luciferase–expressing MDA-MB-231 cells resulted in lung metastases positive for P-selectin expression in the associated vasculature (Fig. 4, A and B).

Because melanoma shows little sensitivity to paclitaxel, we compared the antitumor effects of fucoidan-encapsulated doxorubicin (FiDOX) nanoparticles to the passively targeted DexDOX nanoparticle control and drug-polymer conjugate, DPD, at equivalent doxorubicin doses of 8 mg/kg in the B16F10 model. The mean survival of the FiDOX group was significantly higher (68.8 days) with 40% complete and durable responses, compared to DexDOX (40.2 days) with no complete responses, DPD (39.2 days), or untreated controls (32.4 days) (Fig. 4C; log-rank test $z = 3.11$, $P = 0.00184$).

Author Manuscript Author Manuscript Author Manuscript Author Manuscript

To investigate whether FiDOX nanoparticles exhibited an improved therapeutic index over free doxorubicin, we administered three different doses of FiDOX nanoparticles in the B16F10 model. Mice bearing lung metastases were treated with a single dose of free doxorubicin (6 mg/kg), fucoidan (30 mg/kg) as a vehicle control, or FiDOX nanoparticles with several different doses of encapsulated doxorubicin (1, 5, and 30 mg/kg). The dose range explored the potential for both dose reduction due to improved tumor exposure and dose escalation due to reduced systemic exposure. All three FiDOX treatment arms resulted in decreased tumor burden and prolonged survival after a single injection, whereas an equivalent amount of free doxorubicin at its maximum tolerated dose did not have a significant effect, demonstrating the superiority of FiDOX over free doxorubicin (Fig. 4D). The fucoidan-only controls showed no survival benefit. Moreover, tumor bioluminescence 7 days after treatment with FiDOX showed a clear reduction in median photon count in the medium- and high-dose groups (Fig. 4, E and F, and fig. S6A). Similar results were observed in an MDA-MB-231 breast cancer lung metastasis model, which showed a marked reduction of tumor bioluminescence and prolonged survival in FiDOX-treated mice (Fig. 4, G and H, and fig. S6B).

Organ biodistribution studies confirmed that FiDOX nanoparticles accumulated within areas of lung metastases, whereas DexDOX showed less accumulation in these regions (fig. S7A). Immunofluorescence microscopy of tumor tissue, resected 24 hours after treatment, revealed substantial increases in both tumor and EC apoptosis in FiDOX-treated mice (fig. S7B). We did not observe any notable signs of toxicity, as measured by weight loss, compared to the group receiving free doxorubicin (fig. S7C). Complete blood count showed no deviations from the normal range (table S2). A cytokine profile showed a slight increase 5 hours after FiDOX administration, and it reverted to baseline by 24 hours (fig. S8).

P-selectin–targeted delivery of MEK/ERK inhibitors

We investigated whether P-selectin–targeted delivery could improve the therapeutic efficacy of kinase inhibitors. The MAPK/ERK pathway is frequently hyperactive in several cancer types including melanoma, colorectal, and lung cancers (38). Several reversible MEK/ERK inhibitors are in clinical trials for RAS- and BRAF-mutated cancers; however, they have dose-limiting toxicities, including severe rash and chronic serous retinopathy (39). Chronic administration is needed because of the temporary nature of the target inhibition (40). We hypothesized that delivery of a MEK inhibitor to the tumor microenvironment using P-selectin–targeted nanoparticles might increase drug exposure to tumor cells and prolong the duration of local inhibition while reducing systemic toxicities. We thus encapsulated the MEK inhibitor MEK162 (41) in fucoidan-based nanoparticles (FiMEK) (as shown in Fig. 1D) to test this hypothesis. In vitro, the FiMEK nanoparticles exhibited almost identical biochemical and antitumor activities as free MEK162 against BRAF-mutated melanoma (A375) and KRAS G12S homozygous mutant lung (A549) cancer cells (Fig. 5A).

In vivo, FiMEK nanoparticles and free MEK162 were administered to mice bearing HCT116 and SW620 tumors, which express P-selectin in the vasculature (fig. S9A). We observed that the nanoparticles accumulated in tumors (fig. S9B) and that weekly FiMEK treatment resulted in enhanced efficacy as compared to a weekly dose of free MEK162 and

Author Manuscript Author Manuscript Author Manuscript Author Manuscript

comparable efficacy to daily administration of the free drug (Fig. 5B and fig. S9C). These results were further validated in vivo using two additional models, LOVO and HCT116, both colorectal xenografts (fig. S9D).

ERK phosphorylation, measured to benchmark MEK activity, was inhibited similarly by both treatments after 2 hours, but significant ($P = 0.0089$) inhibition was maintained at the 16-hour time point only in mice treated with FiMEK (Fig. 5C). Apoptosis was assessed by IHC staining for cleaved PARP [poly(adenosine diphosphate–ribose) polymerase] and TUNEL in HCT116 xenografts treated with MEK162 and FiMEK. PARP and caspase 3 cleavage (Fig. 5, C and D) as well as TUNEL staining (fig. S9E) at 16 hours after treatment were significantly higher ($P = 0.0053$ for PARP cleavage) in the tumors treated with FiMEK.

Because the primary dose-limiting side effect of systemic MEK inhibition in humans is severe skin rash, we assessed MEK inhibition in both tumors and skin (42). To benchmark MEK inhibition, we measured the phosphorylation status of the downstream effector ERK at several time points. Administration of MEK162 inhibited ERK phosphorylation in the skin and tumor at 4 hours, but phosphorylation returned in both tissues after 24 hours. The FiMEK nanoparticles elicited prolonged pERK inhibition in the tumor after 24 hours but minimal inhibition in the skin at either time point (fig. S10). To investigate these findings further, we compared the standard 30 mg/kg dose of MEK162 with 300 mg/kg. We found pERK inhibition in both tumor and skin using the 300 mg/kg dose of free drug at 24 hours, whereas administration of FiMEK at $^{1}/_{10}$ of the MEK162 dose induced superior inhibition in the tumor with minimal inhibition in the skin (Fig. 5E).

DISCUSSION

This study explored the role of P-selectin as a target for cancer drug delivery. We found that P-selectin is expressed on cancer cells of many human tumors and on the tumor-associated vasculature. Although other endothelial-specific adhesion molecules, such as ICAM-1, VCAM-1, CD31/PECAM-1, and VE-cadherin, were previously reported to be expressed on tumor cells of various cancer types and are often associated with increased metastasis and poor patient prognosis (43–45), we found only one previous report describing P-selectin expression on cancer cells—in a metastatic pancreatic tumor cell line (46). Because of the high prevalence of P-selectin in the microenvironments of human tumors and metastases, as evinced by IHC staining, we surmised that targeting P-selectin may improve drug delivery to this environment.

The EPR effect is known to facilitate nanoparticle accumulation in tumor sites of many cancer models (4, 6). The vast majority of tumor models, including the 3LL model and others used herein (47, 48), exhibit EPR-mediated (passive) accumulation, which complicates efforts to assess the additional effects of targeting strategies. To discern the accumulation of nanoparticles by P-selectin targeting versus the EPR effect, we chose to target P-selectin with the polysaccharide fucoidan by using it as both a scaffold for drug encapsulation and a targeting agent. Fucoidan was used successfully in previous studies for imaging P-selectin in mouse models of inflammation (24–29). Control nanoparticles were synthesized identically, except that dextran sulfate was used as the scaffold instead of

Author Manuscript Author Manuscript Author Manuscript Author Manuscript

fucoidan. The resulting nanoparticles were of the same size, surface charge, and drug content as the targeted nanoparticles, but they did not exhibit affinity to P-selectin. This control was also used for multiple antitumor efficacy studies. In all cases, the targeting of P-selectin mediated tumor-specific localization and improved efficacy over passively targeted nanoparticles. However, studies in models that do not exhibit EPR are needed to accurately quantify the net benefit of targeting strategies.

Using a Transwell assay, we conducted in vitro experiments to mimic the biological barriers in the tumor microenvironment. The nanoparticles exhibited an increase in transport through the endothelial monolayer when activated by TNFα. It is known that TNFα induces EC activation, apoptosis, and dysfunction (49). A potential explanation may be increased paracellular diffusion through the endothelial layer (50). However, the increased transport of fucoidan-based versus dextran-based nanoparticles warrants further examination.

Biodistribution studies of the fucoidan-based nanoparticles in mice bearing P-selectin–expressing tumors found selective tumor accumulation within 24 hours after injection. Apart from the tumors, the organs exhibiting nanoparticle accumulation were the lungs and the liver, with virtually no uptake in the spleen. Although nanoparticles often accumulate in the liver and spleen, often before hepatobiliary clearance, it was previously found that the use of endothelial targets can modulate nanoparticle biodistribution to the lungs, likely due to the large endothelial component in this organ (51).

Radiation-based guidance of nanoparticles is an appealing strategy to target tumors given the ubiquitous use of radiotherapy in cancer treatment protocols (19). Radiation can be accurately delivered selectively to tumors while sparing surrounding nonmalignant tissues (52, 53). When used at low doses for short periods of time, radiation therapy is associated with relatively mild adverse effects (54). Because the endogenous overexpression of P-selectin appears to vary substantially among tumor types and patients, we investigated the use of ionizing radiation to induce P-selectin expression as a strategy to present the target in a desired location within the body. In a tumor model that does not express P-selectin, we demonstrated that radiation increases endothelial P-selectin expression and particle accumulation, resulting in antitumor efficacy.

The initial observation of P-selectin translocation/induction by radiation was first reported by Hallahan and Virudachalam (16), Hallahan et al. (17), Corso et al. (18), and Wang and Tepper (19), whose studies suggested the involvement of microtubulin. This work was later followed by reports showing the targeting of a P-selectin antibody to irradiated lung cancer tumors (16, 17). Those findings agree with our nanoparticle data in the same tumor model. Our additional finding of P-selectin expression in the nonirradiated tumor within an irradiated mouse prompts questions of how this phenomenon occurs and whether it is important for treatment strategies. An apparently similar phenomenon, radiotherapy-induced distant immune activation, known as the abscopal effect, has not been studied in the context of P-selectin (35, 55).

One of the most important goals for nanoparticle carriers is the treatment of metastatic disease. From our studies on B16F10 melanoma and MDA-MB-231 metastatic models, it is

Author Manuscript Author Manuscript Author Manuscript Author Manuscript

apparent that P-selectin targeting improved local drug delivery to multiple metastatic sites within the lungs. We identified a clear therapeutic benefit of drug-encapsulated P-selectin–targeted particles, compared to passively targeted drug carriers or a fucoidan polymer control. However, further in-depth studies are needed to measure the differential drug localization within tumor versus nontumor tissues.

Inhibitors of the MEK/ERK pathway, like other drugs targeted to tumor signaling pathways, are promising for their selectivity. Challenges with these forms of therapy include the transient inhibition of their targets, side effects of target inhibition in nontumor tissues, and additional toxicities when administered in combination with other therapeutic agents (42). Such problems may be addressed by the use of a targeted drug carrier to improve the tumor localization of these agents (56). By delivering a MEK inhibitor in a P-selectin–targeted nanoparticle, we found improved efficacy over the free drug with a similar dosing schedule, without apparent MEK inhibition in the skin—a common target organ of clinical side effects. By comparing efficacy of nanoparticles to high doses of free drug, we conclude that the mechanism of prolonged tumor inhibition is the elevation of drug concentration in the tumor resulting from nanoparticle-mediated delivery. In addition, the finding of pERK inhibition in the tumor suggests that the nanoparticle reached not just the ECs in the tumor microenvironment but the cancer cells as well.

It is not yet known whether P-selectin associated with the ECs or tumor cells may be most important for effecting a clinical benefit. Here, we predominantly studied endothelial P-selectin because of the wide availability of models with endothelial expression and the ability to modulate endothelial expression by ionizing radiation. The importance of P-selectin expression on tumor cells for drug delivery purposes would depend on accessibility of the target to the delivery vehicle (mediated by vehicle size), permeability of the endothelium, and the morphology of the tumor microenvironment. Further investigations of this issue are warranted.

In conclusion, we identified P-selectin as a target for tumor-selective drug delivery. The high affinity of fucoidan for P-selectin was exploited to deliver locally therapeutically effective doses of these compounds, avoiding potentially toxic systemic drug exposure. This approach was generalizable across a wide range of tumor types and pharmacophores. We also envision that this platform could be applied to other conditions including vascular and autoimmune diseases.

MATERIALS AND METHODS

Study design

The purpose of this study was to assess P-selectin as a drug delivery target for nanoparticle therapeutics. P-selectin expression in human and animal tissues was measured by IHC. Experiments with cells in culture, tumor spheroids, and murine xenograft models were conducted in a controlled and nonblinded manner. Quantitative measurements of drug carrier targeting were compared to an untargeted control nanoparticle. Antitumor efficacy and side effects of targeted nanoparticles containing several drugs, including paclitaxel, doxorubicin, and MEK162, were compared to untargeted, drug-loaded nanoparticles and the un-

Author Manuscript Author Manuscript Author Manuscript Author Manuscript

encapsulated compounds. The number of animals in each group was determined on the basis of previous studies (56). Host mice carrying xenografts were randomly and equally assigned to either control or treatment groups. Analysis of drug function in tumors was conducted by measurements of pERK inhibition and apoptosis via Western blot and IHC.

Staining of tissue microarrays

Normal and tumor tissue microarrays (TMAs) were obtained from US Biomax Inc. Sections were denoted as follows: BR1002 (breast), LYM1502 (lymphoma), BC041115 (lung), OVC96211 (ovarian), and MT801023 (metastases). The TMAs were deparaffinized with EZ Prep buffer (Ventana Medical Systems). Antigen retrieval was performed with CC1 buffer (Ventana Medical Systems), and sections were blocked for 30 min with Background Buster solution (Innovex) or 10% normal rabbit serum in PBS (for P-selectin staining). Slides were incubated with antibodies against P-selectin (R&D Systems, cat. #AF737, 5 μg/ml) for 5 hours, followed by 60 min of incubation with biotinylated rabbit anti-goat immunoglobulin G (IgG) (Vector, cat. #BA-5000) at 1:200 dilution.

Preparation of DPD polymer

Ten milligrams of homobifunctional hydrazide–PEG–hydrazide (NH_2NH-PEG-$NHNH_2$) polymer (molecular weight, 3400 g/mol; Nanocs) and 10 mg of doxorubicin were dissolved in 3 ml of methanol containing 100 μl of glacial acetic acid. The mixture was stirred in the dark for 24 hours and slowly precipitated in cold acetone/ether (2:1), centrifuged (15,000*g*, 20 min), and dried with vacuum. The product, DPD, was purified with a Sephadex G-25 PD-10 desalting column with water as eluent and lyophilized.

Preparation of FiDOX and DexDOX nanoparticles

Fucoidan from *Fucus vesiculosus* (20 to 300 kD; Sigma) and DPD were dissolved in double-distilled water and mixed at a weight ratio of 1:1, forming gel aggregates. The aggregates were collected after centrifugation (15,000*g*, 10 min) and resuspended in PBS containing excess fucoidan (5:1). The mixture was sonicated with a probe tip ultrasonicator (Sonics & Materials) at 40% intensity for 10 s until a clear dark red solution appeared. The material was pelleted by centrifugation (30,000*g*, 30 min), resuspended in PBS, and sonicated in a bath sonicator for 10 min. Encapsulation efficiency was quantified by UV-Vis spectrophotometer (Jasco, V-670) measurement of the supernatant.

Preparation of FiPAX and DexPAX nanoparticles

Paclitaxel (0.1 ml) dissolved in dimethyl sulfoxide (DMSO) (10 mg/ml) was added drop-wise (20 μl per 15 s) to a 0.6-ml aqueous polysaccharide solution (15 mg/ml) containing IR-783 (1 mg/ml) and 0.05 mM sodium bicarbonate. The solution was centrifuged twice (20,000g, 30 min) and resuspended in 1 ml of sterile PBS. The suspension was sonicated for 10 s with a probe tip ultrasonicator at 40% intensity. The nanoparticles were lyophilized in a 5% saline/sucrose solution. Encapsulation efficiency was quantified by UV-Vis spectrophotometer measurement of the supernatant.

Author Manuscript Author Manuscript Author Manuscript Author Manuscript

Nanoparticle characterization

Dynamic light scattering (DLS) and ζ potential measurements were conducted in PBS using a Zetasizer Nano ZS (Malvern). SEM was conducted using a Zeiss Supra 25 field emission scanning electron microscope. Samples were prepared by gold sputtering and critical point drying.

Drug release measurements

Nanoparticles were incubated in PBS at pH 5.5 or 7.4 at 37°C with a concentration equivalent to 1 μM of the drug. The amount of released drug was determined by extracting into ethanol and measuring absorbance at 260 or 492 nm using a UV-Vis spectrophotometer or plate reader (Tecan, Infinite M1000). All experiments were carried out in duplicate.

Binding studies of nanoparticles to immobilized P-selectin

Human recombinant P-selectin, E-selectin, or L-selectin (50 ng in 50 μl) was added to high hydrophobicity 96-well enzyme-linked immunosorbent assay (ELISA) plates and incubated at 4°C overnight. The wells were washed with PBS and incubated with BSA (3%, 0.2 ml) and with FiPAX or DexPAX in Hank's balanced salt solution (HBSS) for 15 min. The wells were gently washed three times with HBSS. Fluorescence was measured with a plate reader (Tecan, Infinite M1000) by averaging 16 reads per well (excitation, 780 nm/emission, 820 nm).

Binding of nanoparticles to P-selectin–expressing ECs

bEnd.3 EC monolayers in 24-well plates were preincubated with TNFα (50 ng/ml) for 20 min before adding nanoparticles. Control cells were left untreated. The cells were then incubated with nanoparticles (20 μg/ml) for 45 min and for another 15 min with CellMask Green (Life Technologies) for membrane staining and with Hoechst 33342 (Life Technologies) for nuclear staining. The cells were rinsed twice with PBS. A similar method was used for the binding of nanoparticles to irradiated cells. Irradiation of cultured cells was carried out in Shepherd Mark I irradiator containing a ^{137}Cs source at a rate of 2.08 Gy/min. Images were acquired with an inverted Olympus IX51 fluorescence microscope equipped with XM10IR Olympus camera and Excite Xenon lamp. Similar exposure times and excitation intensities were applied throughout all experiments. Filter sets: cell membrane (excitation, 488 nm/emission, 525 nm), nucleus (excitation, 350 nm/emission, 460 nm), IR-783 dye in particles (excitation, 780 nm/emission, 820 nm). Images were processed with ImageJ software.

Development of tumor spheroids

To generate P-selectin–expressing multicellular tumor spheroids, we developed a murine cell line, SK-136, derived from an autochthonous model of liver cancer. To generate liver tumors, we performed hydrodynamic transfection as described previously (57). Specifically, 10 μg of pT3-EF1a-c-myc, 10 μg of pT3-EF1a-β-cateninT41A–IRES-GFP, and CMV-SB13 Sleeping Beauty transposase were mixed in sterile saline solution. A total volume of plasmid-saline solution mix corresponding to 10% of the body weight was injected into the lateral tail vein of 6- to 8-week-old female FVB/N mice (Jackson Laboratory) within 5 to 7 s

Author Manuscript Author Manuscript Author Manuscript Author Manuscript

(57). The harvested cells were plated on two ultra-low attachment 96-well plates (Corning) and incubated for 3 days. The wells were examined with an inverted light microscope to identify the formation of multicellular tumor spheroids. The wells containing tumor spheres were centrifuged, trypsinized, and seeded in 75-cm cell culture–treated flasks with Dulbecco's modified Eagle's medium (DMEM). This process was repeated three times to generate a subclone of spheroid-forming cells. To identify P-selectin expression in 7-day-old tumor spheroids, they were collected at the bottom of an Eppendorf tube, suspended in paraformaldehyde (PFA), and embedded in paraffin. Ten-micrometer slices were stained with anti-mouse P-selectin antibody (R&D Systems). A second tumor spheroid, derived from a PDX of SCLC (designated JHU-LX33), was generated as described previously and grown with complete DMEM supplemented with 10% fetal bovine serum (FBS) with 1% penicillin/streptomycin and 2 mM L-glutamine (34).

Characterization of tumor spheroids

SK-136 cells were grown in ultra-low attachment flasks (Corning) for 5 days. Once the spheres were formed, the medium containing tumor spheres was removed and placed in 1-ml Eppendorf tube. The spheres were allowed to settle by gravity for 2 min, and the medium was replaced with fresh medium. The spheroids were placed on poly-L-lysine–coated plastic coverslips (Thermonex). For SEM imaging, the spheroids were fixed in 2.5% PFA in 0.075 M cacodylate buffer for 1 hour, rinsed in cacodylate buffer, and dehydrated in a graded series of alcohols: 50, 75, 95, and 100%. The samples were then dried in a JCP-1 critical point dryer (Denton). The coverslips were attached to SEM stubs and sputter-coated with gold/palladium using a Desk IV sputter system (Denton Vacuum). The images were obtained in a Zeiss Supra 25 field emission scanning electron microscope. For IHC measurements, the spheroids were embedded, sectioned, and processed for H&E and P-selectin staining as described below.

Binding of nanoparticles to P-selectin–expressing tumor spheroids

SK-136 cells (10^4) were seeded in 25-cm^2 ultra-low attachment flasks (Corning) and grown for 7 days in DMEM with medium replacement every 3 days. When spheres reached a diameter of about 250 μm, 0.2 ml of growth suspension was plated in normal adhesion 96-well plates, yielding three to five spheres per well. After 30 min, spheres adhered to the bottom of the wells. Nanoparticles were added at a concentration of 50 μg/ml and incubated for 20 to 40 min. The wells were washed three times with HBSS buffer and imaged with an inverted Olympus IX51 fluorescence microscope equipped with an XM10 Olympus charge-coupled device camera. The fluorescence intensity was analyzed using ImageJ software.

Evaluation of penetration through endothelial and epithelial barriers

We used a modified Transwell assay (Life Technologies) to test the penetration of nanoparticles through a monolayer of ECs. bEnd.3 cells (5×10^4 in 0.5 ml) were grown on Transwell inserts in 24-well plates for 7 days. The medium was replaced every other day. The confluence of the monolayer was ensured by imaging the cell membrane with CellMask Green. Experiments were conducted in the absence of gaps in cell junctions. After activation with TNFα as described above, the cells were incubated with nanoparticles (20 μg/ml) for 1 hour. Samples of medium from the upper chamber (50 μl) were collected and measured with

Author Manuscript Author Manuscript Author Manuscript Author Manuscript

a fluorescence plate reader (Tecan, Infinite M1000) (excitation, 780 nm/emission, 820 nm). To visualize nanoparticles in the ECs on the insert component of the chamber, the cells were washed twice with PBS and then incubated in HBSS. Images were acquired and processed as described above.

Cell viability assay

bEnd.3 cells (5×10^4) were seeded in a 96-well plate. Cells were activated with TNFα for 30 min. Nanoparticles were added at equivalent drug concentrations for each well and incubated for 1 hour at 37°C Cells not activated with TNFα were treated similarly. The drug solutions were then removed and replaced with fresh medium, followed by 72 hours of incubation at 37°C Cell survival was assayed by discarding the medium and adding 100 μl of fresh medium and 25 μl of MTT solution (5 mg/ml) in PBS to each well. After 90 min, the solution was removed and 200 μl of DMSO was added. Cell viability was evaluated by measuring the absorbance of each well at 570 nm relative to control wells.

Radiation treatment studies in bilateral model of 3LL

Murine Lewis lung carcinoma (3LL) cells were maintained in DMEM supplemented with 10% FBS, 1 mM Na pyruvate, and penicillin/streptomycin (50 μg/ml). Tumor cells were subcutaneously implanted (1×10^6 cells per injection) in both hindlimbs of 8-week-old immunocompetent, hairless SKH-1 mice. The tumor models were used for biodistribution and tumor growth studies when the tumor size reached 0.5 cm in diameter. Irradiation of the tumors was conducted by giving 6-Gy doses using an X-RAD 225 Cx Micro-Irradiator (Precision X-Ray) with a 50-cm source-to-skin distance. Mice were lightly sedated with ketamine (0.1 mg/g) and xylazine (0.02 mg/g). Only tumor, surrounding skin, and subcutaneous tissues were exposed using a specialized lead jig. All of the animal studies were conducted according to the protocols approved by the Memorial Sloan Kettering Cancer Center (MSKCC) Institutional Animal Care and Use Committee.

In vivo imaging for radiotherapy studies

Four hours after irradiation (as described above), 200 μl (1 mg/ml) of the nanoparticles labeled with IR-783 was injected via the tail vein. Images were taken with an IVIS imaging system (Xenogen Corp.). Radiance (photons/s per cm^2) was calculated for the tumor ROI using Living Image V4.2 software.

Detection of sP-selectin in plasma

A sandwich ELISA kit (R&D Systems) was used to quantify sP-selectin in human and mouse serum according to the manufacturer’s instructions.

B16F10 melanoma lung metastasis studies

C57BL/6 mice were inoculated intravenously with 10^5 B16F10 cells expressing luciferase. Tumors were allowed to grow until day 7. In the first experiment, mice were divided randomly into groups and injected intravenously with FiDOX nanoparticles and controls. After treatment, mice were monitored for up to 8 or 17 weeks, depending on the treatment received. Bioluminescence imaging was conducted using an IVIS imager after luciferin

Author Manuscript Author Manuscript Author Manuscript Author Manuscript

injection (50 mg/ml). Mice that lost more than 15% of their body weight were sacrificed using CO_2.

Tumor xenograft studies in nude mice

Six-week-old female athymic NU/NU nude mice purchased from Charles River Laboratories were injected subcutaneously with 5×10^5 of A375, SW620, LOVO, or HCT116 cells in 100-ml culture medium/Matrigel (BD Biosciences) at a ratio of 1:5. Animals were randomized at a tumor volume of 70 to 120 mm^3 into four to six groups, with $n = 8$ to 10 tumors per group. Animals were treated orally daily with MEK162 [10 or 30 mg/kg in 0.5% carboxymethylcellulose sodium salt (Sigma)]. Tumor size was measured with a digital caliper, and tumor volumes were calculated using the following formula: (length × $width^2$) × (π/6). Animals were euthanized using CO_2 inhalation. Mice were housed in air-filtered laminar flow cabinets with a 12-hour light/dark cycle and food and water ad libitum. Mice were maintained and treated in accordance with the institutional guidelines of MSKCC. Animal experiments were approved by MSKCC.

Immunohistochemistry

For xenograft samples, dissected tissues were fixed immediately after removal in a 10% buffered formalin solution for a maximum of 24 hours at room temperature before being dehydrated and paraffin-embedded under vacuum. The tissue sections were deparaffinized with EZ Prep buffer (Ventana Medical Systems). Antigen retrieval was performed with CC1 buffer (Ventana Medical Systems), and sections were blocked for 30 min with Background Buster solution (Innovex).

The IHC detection was performed at the Molecular Cytology Core Facility of MSKCC using DISCOVERY XT processor (Ventana Medical Systems). All the tissues were harvested from mice and were fixed in 4% PFA overnight. Fixed tissues were dehydrated and embedded in paraffin before 5-μm sections were put on slides. The tissue sections were deparaffinized with EZ Prep buffer (Ventana Medical Systems); antigen retrieval was performed with CC1 buffer (Ventana Medical Systems); and sections were blocked for 30 min with Background Buster solution (Innovex) or 10% normal rabbit serum in PBS (for P-selectin staining). P-selectin sections were incubated with antibodies against P-selectin (R&D Systems, cat. #AF737, 5 μg/ml) for 5 hours, followed by 60 min of incubation with biotinylated rabbit anti-goat IgG (Vector, cat #BA-5000) at 1:200 dilution. pMAPK sections were blocked with avidin/biotin block for 12 min, followed by incubation with pMAPK antibodies (Cell Signaling, cat. #4370, 1 μg/ml) for 5 hours, followed by 60 min of incubation with biotinylated goat anti-rabbit IgG (Vector, cat. #PK6101) at 1:200 dilution. Ki67 sections were incubated with Ki67 antibodies (Vector, cat. #VP-K451, 0.4 μg/ml) for 5 hours, followed by 60 min of incubation with biotinylated goat anti-rabbit IgG (Vector, cat #PK6101) at 1:200 dilution. CD31 sections were incubated with CD31 antibodies (Dianova, cat. #DIA-310, 1 μg/ml) for 5 hours, followed by 60 min of incubation with biotinylated rabbit anti-rat IgG (Vector, cat. #PK-4004) at 1:200 dilution. Detection was performed with a DAB detection kit (Ventana Medical Systems) according to the manufacturer's instructions, followed by counterstaining with hematoxylin (Ventana Medical Systems) and coverslipping with Permount (Fisher Scientific).

Author Manuscript Author Manuscript Author Manuscript Author Manuscript

Statistics

Statistical analysis for in vitro and in vivo experiments was performed using GraphPad Prism (GraphPad Software). A two-tailed Student's unpaired *t* test was performed to compare control versus treated groups. The significance level was set at $P < 0.05$. Independent experiments were conducted with a minimum of two biological replicates per condition to allow for statistical comparison. Error bars represent the SEM, and *P* values are indicated. All cellular experiments were repeated at least two times. Survival plots of experimental metastasis models were analyzed using the Mantel-Cox log-rank test.

Supplementary Material

Refer to Web version on PubMed Central for supplementary material.

Acknowledgments

We would like to thank the following core facilities at MSKCC: Molecular Cytology, Electron Microscopy, Small Animal Imaging, and Antitumor Assessment. We would like to thank N. Lampen for assistance with electron microscopy. We would also like to thank J. Budhathoki-Uprety, R. Williams, J. Harvey, D. Roxbury, T. Galassi, J. Humm, and C. Horoszko for helpful discussions. **Funding:** This work was supported by the NIH Director's New Innovator Award (DP2-HD075698), the Cancer Center Support Grant (P30-CA008748), the Experimental Therapeutics Center, Mr. William H. Goodwin and Mrs. Alice Goodwin and the Commonwealth Foundation for Cancer Research, the Alan and Sandra Gerry Metastasis Research Initiative, the Imaging and Radiation Sciences Program, Cycle for Survival, the Louis V. Gerstner Jr. Young Investigator's Fund, the Honorable Tina Brozman Foundation for Ovarian Cancer Research, the Anna Fuller Fund, the Frank A. Howard Scholars Program, and the Center for Molecular Imaging and Nanotechnology at MSKCC. M.E. is an International Sephardic Education Foundation postdoctoral fellow.

REFERENCES AND NOTES

1. Chow EK-H, Ho D. Cancer nanomedicine: From drug delivery to imaging. Sci. Transl. Med. 2013; 5:216rv4.
2. Ferrari M. Cancer nanotechnology: Opportunities and challenges. Nat. Rev. Cancer. 2005; 5:161–171. [PubMed: 15738981]
3. Lammers T, Kiessling F, Hennink WE, Storm G. Drug targeting to tumors: Principles, pitfalls and (pre-) clinical progress. J Control. Release. 2012; 161:175–187. [PubMed: 21945285]
4. Prabhakar U, Maeda H, Jain RK, Sevick-Muraca EM, Zamboni W, Farokhzad OC, Barry ST, Gabizon A, Grodzinski P, Blakey DC. Challenges and key considerations of the enhanced permeability and retention effect for nanomedicine drug delivery in oncology. Cancer Res. 2013; 73:2412–2417. [PubMed: 23423979]
5. Grodzinski P, Farrell D. Future opportunities in cancer nanotechnology—NCI strategic workshop report. Cancer Res. 2014; 74:1307–1310. [PubMed: 24413533]
6. Matsumura Y, Maeda H. A new concept for macromolecular therapeutics in cancer chemotherapy: Mechanism of tumoritropic accumulation of proteins and the antitumor agent smancs. Cancer Res. 1986; 46:6387–6392. [PubMed: 2946403]
7. O'Brien MER, Wigler N, Inbar M, Rosso R, Grischke E, Santoro A, Catane R, Kieback DG, Tomczak P, Ackland SP, Orlandi F, Mellars L, Alland L, Tendler C. Reduced cardiotoxicity and comparable efficacy in a phase III trial of pegylated liposomal doxorubicin HCl (CAE-LYX™/Doxil®) versus conventional doxorubicin for first-line treatment of metastatic breast cancer. Ann. Oncol. 2004; 15:440–449. [PubMed: 14998846]
8. Curnis F, Sacchi A, Corti A. Improving chemotherapeutic drug penetration in tumors by vascular targeting and barrier alteration. J Clin. Invest. 2002; 110:475–482. [PubMed: 12189241]
9. Hrkach J, Von Hoff D, Mukkaram Ali M, Andrianova E, Auer J, Campbell T, De Witt D, Figa M, Figueiredo M, Horhota A, Low S, McDonnell K, Peeke E, Retnarajan B, Sabnis A, Schnipper E, Song JJ, Ho Song Y, Summa J, Tompsett D, Troiano G, Van Geen Hoven T, Wright J, LoRusso P,

Author Manuscript Author Manuscript Author Manuscript Author Manuscript

Kantoff PW, Bander NH, Sweeney C, Farokhzad OC, Langer R, Zale S. Preclinical development and clinical translation of a PSMA-targeted docetaxel nanoparticle with a differentiated pharmacological profile. Sci. Transl. Med. 2012; 4:128ra39.

10. Schroeder A, Heller DA, Winslow MM, Dahlman JE, Pratt GW, Langer R, Jacks T, Anderson DG. Treating metastatic cancer with nanotechnology. Nat. Rev. Cancer. 2011; 12:39–50. [PubMed: 22193407]
11. Kansas GS. Selectins and their ligands: Current concepts and controversies. Blood. 1996; 88:3259–3287. [PubMed: 8896391]
12. Läubli H, Borsig L. Selectins promote tumor metastasis. Semin. Cancer Biol. 2010; 20:169–177. [PubMed: 20452433]
13. Erpenbeck L, Schön MP. Deadly allies: The fatal interplay between platelets and metastasizing cancer cells. Blood. 2010; 115:3427–3436. [PubMed: 20194899]
14. Amano H, Ito Y, Ogawa F, Eshima K, Suzuki T, Oba K, Matsui Y, Kato S, Fukui T, Nakamura M, Kitasato H, Fukamizu A, Majima M. Angiotensin II type 1A receptor signaling facilitates tumor metastasis formation through P-selectin–Mediated interaction of tumor cells with platelets and endothelial cells. Am. J. Pathol. 2013; 182:553–564. [PubMed: 23219751]
15. Bonfanti R, Furie BC, Furie B, Wagner DD. PADGEM (GMP140) is a component of Weibel-Palade bodies of human endothelial cells. Blood. 1989; 73:1109–1112. [PubMed: 2467701]
16. Hallahan DE, Virudachalam S. Accumulation of P-selectin in the lumen of irradiated blood vessels. Radiat. Res. 1999; 152:6–13. [PubMed: 10381836]
17. Hallahan DE, Staba-Hogan MJ, Virudachalam S, Kolchinsky A. X-ray-induced P-selectin localization to the lumen of tumor blood vessels. Cancer Res. 1998; 58:5216–5220. [PubMed: 9823335]
18. Corso CD, Ali AN, Diaz R. Radiation-induced tumor neoantigens: Imaging and therapeutic implications. Am. J. Cancer Res. 2011; 1:390–412. [PubMed: 21969260]
19. Wang AZ, Tepper JE. Nanotechnology in radiation oncology. J Clin. Oncol. 2014; 32:2879–2885. [PubMed: 25113769]
20. Gong L, Mi H-J, Zhu H, Zhou X, Yang H. P-selectin-mediated platelet activation promotes adhesion of non-small cell lung carcinoma cells on vascular endothelial cells under flow. Mol. Med. Rep. 2012; 5:935–942. [PubMed: 22266541]
21. Gunningham SP, Currie MJ, Morrin HR, Tan EY, Turley H, Dachs GU, Watson AI, Frampton C, Robinson BA, Fox SB. The angiogenic factor thymidine phosphorylase up-regulates the cell adhesion molecule P-selectin in human vascular endothelial cells and is associated with P-selectin expression in breast cancers. J Pathol. 2007; 212:335–344. [PubMed: 17487938]
22. Hemmerlein B, Scherbening J, Kugler A, Radzun H-J. Expression of VCAM-1, ICAM-1, E- and P-selectin and tumour-associated macrophages in renal cell carcinoma. Histopathology. 2000; 37:78–83. [PubMed: 10931222]
23. Hariri G, Zhang Y, Fu A, Han Z, Brechbiel M, Tantawy MN, Peterson TE, Mernaugh R, Hallahan D. Radiation-guided P-selectin antibody targeted to lung cancer. Ann. Biomed. Eng. 2008; 36:821–830. [PubMed: 18273706]
24. Rouzet F, Bachelet-Violette L, Alsac J-M, Suzuki M, Meulemans A, Louedec L, Petiet A, Jandrot-Perrus M, Chaubet F, Michel J-B, Le Guludec D, Letourneur D. Radiolabeled fucoidan as a p-selectin targeting agent for in vivo imaging of platelet-rich thrombus and endothelial activation. J Nucl. Med. 2011; 52:1433–1440. [PubMed: 21849401]
25. Bachelet L, Bertholon I, Lavigne D, Vassy R, Jandrot-Perrus M, Chaubet F, Letourneur D. Affinity of low molecular weight fucoidan for P-selectin triggers its binding to activated human platelets. Biochim. Biophys. Acta. 2009; 1790:141–146. [PubMed: 19026722]
26. Li X, Bauer W, Israel I, Kreissl MC, Weirather J, Richter D, Bauer E, Herold V, Jakob P, Buck A, Frantz S, Samnick S. Targeting P-selectin by gallium-68–labeled fucoidan positron emission tomography for noninvasive characterization of vulnerable plaques: Correlation with in vivo 17.6T MRI. Arterioscler. Thromb. Vasc. Biol. 2014; 34:1661–1667. [PubMed: 24903095]
27. Bonnard T, Yang G, Petiet A, Ollivier V, Haddad O, Arnaud D, Louedec L, Bachelet-Violette L, Derkaoui SM, Letourneur D, Chauvierre C, Le Visage C. Abdominal aortic aneurysms targeted by

Author Manuscript Author Manuscript Author Manuscript Author Manuscript

functionalized polysaccharide microparticles: A new tool for SPECT imaging. Theranostics. 2014; 4:592–603. [PubMed: 24723981]

28. Bonnard T, Serfaty J-M, Journé C, Ho Tin Noe B, Arnaud D, Louedec L, Derkaoui SM, Letourneur D, Chauvierre C, Le Visage C. Leukocyte mimetic polysaccharide microparticles tracked in vivo on activated endothelium and in abdominal aortic aneurysm. Acta Biomater. 2014; 10:3535–3545. [PubMed: 24769117]
29. Carvalho ACS, Sousa RB, Franco ÁX, Costa JVG, Neves LM, Ribeiro RA, Sutton R, Criddle DN, Soares PMG, de Souza MHLP. Protective effects of fucoidan, a P- and L-selectin inhibitor, in murine acute pancreatitis. Pancreas. 2014; 43:82–87. [PubMed: 24177139]
30. Jena PV, Shamay Y, Shah J, Roxbury D, Paknejad N, Heller DA. Photoluminescent carbon nanotubes interrogate the permeability of multicellular tumor spheroids. Carbon. 2016; 97:99–109. [PubMed: 26456974]
31. Pan J, Xia L, Yao L, McEver RP. Tumor necrosis factor-α- or lipopolysaccharide-induced expression of the murine P-selectin gene in endothelial cells involves novel κB sites and a variant activating transcription factor/cAMP response element. J Biol. Chem. 1998; 273:10068–10077. [PubMed: 9545354]
32. Parodi A, Quattrocchi N, van de Ven AL, Chiappini C, Evangelopoulos M, Martinez JO, Brown BS, Khaled SZ, Yazdi IK, Enzo MV, Isenhart L, Ferrari M, Tasciotti E. Synthetic nanoparticles functionalized with biomimetic leukocyte membranes possess cell-like functions. Nat. Nanotechnol. 2013; 8:61–68. [PubMed: 23241654]
33. Yuan W, Li G, Fu BM. Effect of surface charge of immortalized mouse cerebral endothelial cell monolayer on transport of charged solutes. Ann. Biomed. Eng. 2010; 38:1463–1472. [PubMed: 20087768]
34. Daniel VC, Marchionni L, Hierman JS, Rhodes JT, Devereux WL, Rudin CM, Yung R, Parmigiani G, Dorsch M, Peacock CD, Watkins DN. A primary xenograft model of small-cell lung cancer reveals irreversible changes in gene expression imposed by culture in vitro. Cancer Res. 2009; 69:3364–3373. [PubMed: 19351829]
35. Siva S, MacManus MP, Martin RF, Martin OA. Abscopal effects of radiation therapy: A clinical review for the radiobiologist. Cancer Lett. 2015; 356:82–90. [PubMed: 24125863]
36. Poste G, Doll J, Fidler IJ. Interactions among clonal subpopulations affect stability of the metastatic phenotype in polyclonal populations of B16 melanoma cells. Proc. Natl. Acad. Sci. U.S.A. 1981; 78:6226–6230. [PubMed: 6947225]
37. Minn AJ, Gupta GP, Siegel PM, Bos PD, Shu W, Giri DD, Viale A, Olshen AB, Gerald WL, Massagué J. Genes that mediate breast cancer metastasis to lung. Nature. 2005; 436:518–524. [PubMed: 16049480]
38. Fernández-Medarde A, Santos E. Ras in cancer and developmental diseases. Genes Cancer. 2011; 2:344–358. [PubMed: 21779504]
39. Wang D, Boerner SA, Winkler JD, LoRusso PM. Clinical experience of MEK inhibitors in cancer therapy. Biochim. Biophys. Acta. 2007; 1773:1248–1255. [PubMed: 17194493]
40. Frémin C, Meloche S. From basic research to clinical development of MEK1/2 inhibitors for cancer therapy. J Hematol. Oncol. 2010; 3:8. [PubMed: 20149254]
41. Ascierto PA, Schadendorf D, Berking C, Agarwala SS, van Herpen CML, Queirolo P, Blank CU, Hauschild A, Beck JT, St-Pierre A, Niazi F, Wandel S, Peters M, Zubel A, Dummer R. MEK162 for patients with advanced melanoma harbouring *NRAS* or Val600 *BRAF* mutations: A non-randomised, open-label phase 2 study. Lancet Oncol. 2013; 14:249–256. [PubMed: 23414587]
42. Catalanotti F, Solit DB, Pulitzer MP, Berger MF, Scott SN, Iyriboz T, Lacouture ME, Panageas KS, Wolchok JD, Carvajal RD, Schwartz GK, Rosen N, Chapman PB. Phase II trial of MEK inhibitor selumetinib (AZD6244, ARRY-142886) in patients with $BRAF^{V600E/K}$-mutated melanoma. Clin. Cancer Res. 2013; 19:2257–2264. [PubMed: 23444215]
43. Rosette C, Roth RB, Oeth P, Braun A, Kammerer S, Ekblom J, Denissenko MF. Role of ICAM1 in invasion of human breast cancer cells. Carcinogenesis. 2005; 26:943–950. [PubMed: 15774488]
44. Chen Q, Zhang XH-F, Massagué J. Macrophage binding to receptor VCAM-1 transmits survival signals in breast cancer cells that invade the lungs. Cancer Cell. 2011; 20:538–549. [PubMed: 22014578]

Author Manuscript Author Manuscript Author Manuscript Author Manuscript

45. Righi L, Deaglio S, Pecchioni C, Gregorini A, Horenstein AL, Bussolati G, Sapino A, Malavasi F. Role of CD31/platelet endothelial cell adhesion molecule-1 expression in in vitro and in vivo growth and differentiation of human breast cancer cells. Am. J. Pathol. 2003; 162:1163–1174. [PubMed: 12651608]

46. Iwamura T, Caifrey TC, Kitamura N, Yamanan H, Setoguchi T, Hoffingsworth MA. P-selectin expression in a metastatic pancreatic tumor cell line (SUIT-2). Cancer Res. 1997; 57:1206–1212. [PubMed: 9067294]

47. Lukyanov AN, Gao Z, Mazzola L, Torchilin VP. Polyethylene glycol-diacyllipid micelles demonstrate increased acculumation in subcutaneous tumors in mice. Pharm. Res. 2002; 19:1424–1429. [PubMed: 12425458]

48. Lv P-P, Wei W, Yue H, Yang T-Y, Wang L-Y, Ma G-H. Porous quaternized chitosan nanoparticles containing paclitaxel nanocrystals improved therapeutic efficacy in non-small-cell lung cancer after oral administration. Biomacromolecules. 2011; 12:4230–4239. [PubMed: 22044456]

49. Verheij M, Bose R, Hua Lin X, Yao B, Jarvis WD, Grant S, Birrer MJ, Szabo E, Zon LI, Kyriakis JM, Haimovitz-Friedman A, Fuks Z, Kolesnick RN. Requirement for ceramide-initiated SAPK/JNK signalling in stress-induced apoptosis. Nature. 1996; 380:75–79. [PubMed: 8598911]

50. Mark KS, Miller DW. Increased permeability of primary cultured brain microvessel endothelial cell monolayers following TNF-α exposure. Life Sci. 1999; 64:1941–1953. [PubMed: 10353592]

51. Shuvaev VV, Brenner JS, Muzykantov VR. Targeted endothelial nanomedicine for common acute pathological conditions. J Control. Release. 2015; 219:576–595. [PubMed: 26435455]

52. Okunieff P, Morgan D, Niemierko A, Suit HD. Radiation dose-response of human tumors. Int. J. Radiat. Oncol. Biol. Phys. 1995; 32:1227–1237. [PubMed: 7607946]

53. Bernier J, Hall EJ, Giaccia A. Radiation oncology: A century of achievements. Nat. Rev. Cancer. 2004; 4:737–747. [PubMed: 15343280]

54. Prise KM. New advances in radiation biology. Occup. Med. 2006; 56:156–161.

55. Prasanna A, Ahmed MM, Mohiuddin M, Norman Coleman C. Exploiting sensitization windows of opportunity in hyper and hypo-fractionated radiation therapy. J Thorac. Dis. 2014; 6:287–302. [PubMed: 24688774]

56. Dreaden EC, Wen Kong Y, Morton SW, Correa S, Young Choi K, Shopsowitz KE, Renggli K, Drapkin R, Yaffe MB, Hammond PT. Tumor-targeted synergistic blockade of MAPK and PI3K from a layer-by-layer nanoparticle. Clin. Cancer Res. 2015; 21:4410–4419. [PubMed: 26034127]

57. Chow EK-H, Fan L-l, Chen X, Bishop JM. Oncogene-specific formation of chemoresistant murine hepatic cancer stem cells. Hepatology. 2012; 56:1331–1341. [PubMed: 22505225]

Author Manuscript
Author Manuscript
Author Manuscript
Author Manuscript

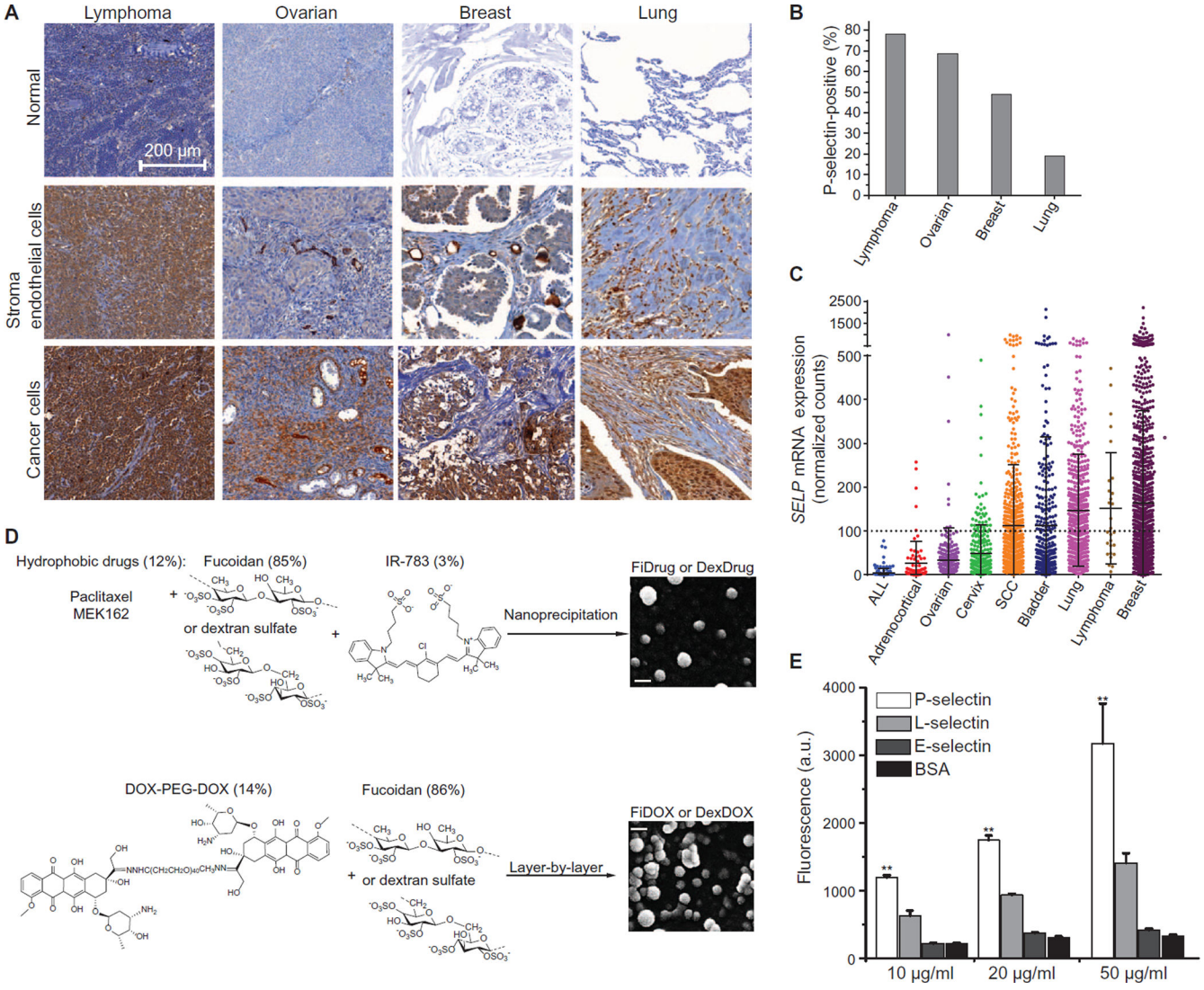

Fig. 1. P-selectin expression in human cancers, preparation of targeted nanoparticles, and binding studies to reconstituted protein

(**A**) Human cancer tissues stained with P-selectin antibody. Lymphoma stroma: non-Hodgkin's B cell lymphoma (lymph node); cancer cells: brain metastases of non-Hodgkin's B cell lymphoma. Ovarian stroma: lymph node metastases of serous papillary adenocarcinoma; cancer cells: endometrioid carcinoma. Breast cancer ECs: infiltrating ductal carcinoma; cancer cells: advanced infiltrating ductal carcinoma. Lung cancer stroma: lung squamous cell carcinoma; cancer cells: small cell undifferentiated carcinoma. (**B**) Percentage of positively stained samples from tumor microarrays. (**C**) *SELP* RNA expression (RNASeq Version 2) in patients from TCGA. A threshold for high expression was set at the highest expression of the lowest expressing cancer. ALL, acute lymphoblastic leukemia; SCC, squamous cell carcinoma. (**D**) Synthesis schemes of P-selectin–targeted nanoparticles. Top: Preparation of fucoidan-encapsulated paclitaxel and MEK162 nanoparticles (FiPAX and FiMEK) and dextran sulfate–encapsulated controls by nanoprecipitation. Bottom: Preparation of fucoidan-encapsulated doxorubicin nanoparticles

Author Manuscript Author Manuscript Author Manuscript Author Manuscript

(FiDOX) and dextran sulfate–encapsulated control (DexDOX) via layer-by-layer assembly. Right: Scanning electron microscopy (SEM) images of FiPAX and FiDOX nanoparticles. Scale bars, 100 nm. (**E**) Binding assay of FiPAX to immobilized recombinant proteins. Error bars are ± SD of the mean ($n = 4$); from left to right, $P = 0.0062$, 0.0028, 0.0022. *$P < 0.05$, **$P < 0.01$. a.u., arbitrary units.

Author Manuscript Author Manuscript Author Manuscript Author Manuscript

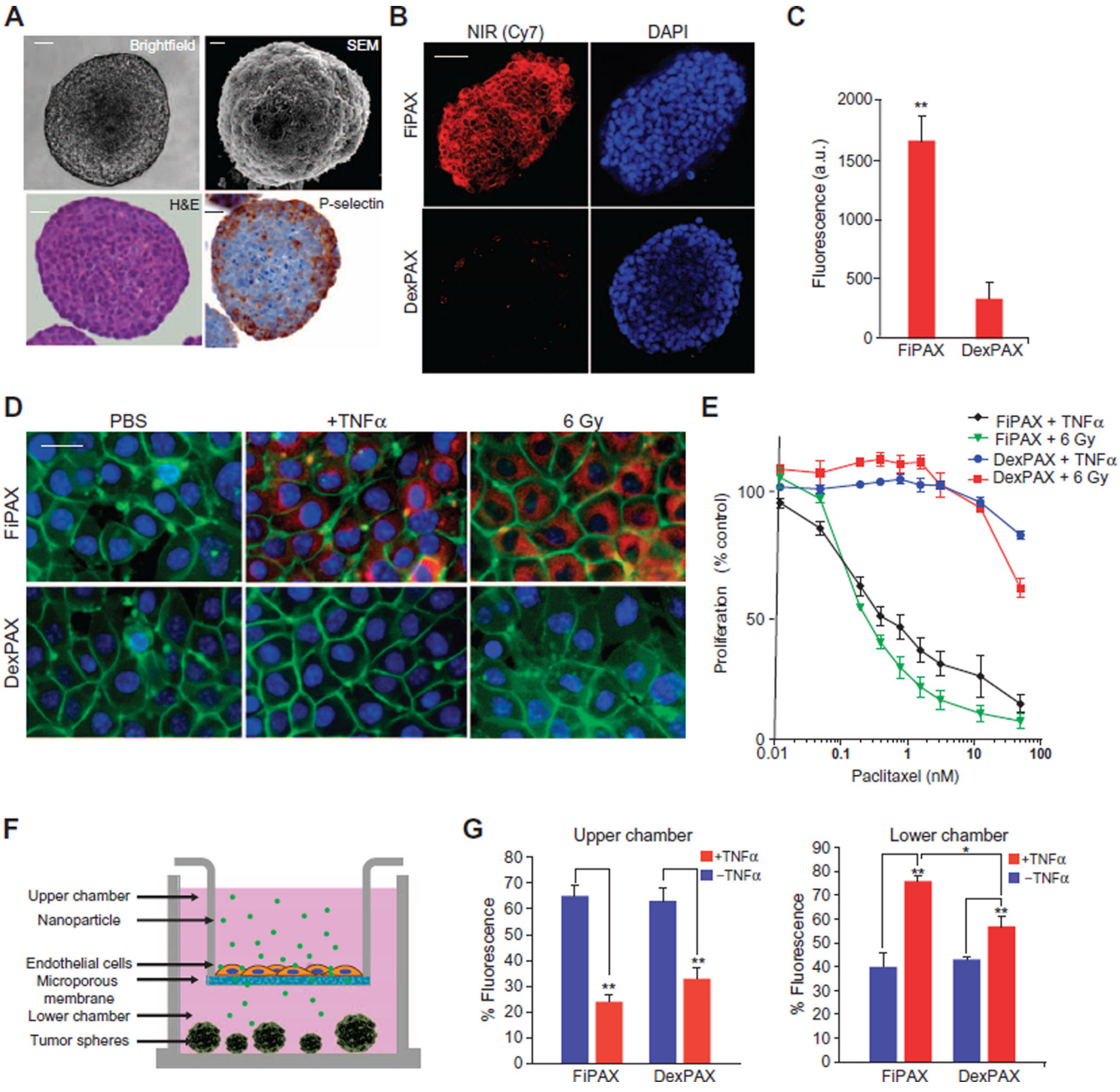

Fig. 2. In vitro studies of nanoparticle penetration of endothelium and tumor

(**A**) Liver tumor spheroid model, SK-136, which constitutively expresses P-selectin at the surface. Top: Bright-field microscopy and SEM. Bottom: Hematoxylin and eosin (H&E) and IHC staining with a P-selectin antibody. Scale bars, 10 μm. (**B**) Fluorescence microscopy of NIR dye emission from nanoparticles in the tumor spheroids. Red, NIR fluorescence; blue, 4′,6-diamidino-2-phenylindole (DAPI) nuclear staining. Scale bar, 20 μm. (**C**) Quantification of nanoparticle emission in tumor spheres. Bars show means ± SD of $n = 6$ spheres; $P = 0.0042$. (**D**) Fluorescence images of human endothelial monolayer (EA.hy926) treated with TNFα and ionizing radiation (6 Gy) to induce P-selectin. Red, NIR dye in FiPAX or control DexPAX nanoparticles; green, CellMask membrane stain; blue, DAPI

Author Manuscript Author Manuscript Author Manuscript Author Manuscript

nuclear stain. Scale bar, 5 μm. (**E**) Nanopartide-mediated cytotoxicity of bEnd.3 cells activated by TNFα or 6 Gy, as measured by MTT (4,5-dimethylthiazol-2-yl)-2,5-diphenyltetrazolium bromide) cell viability assay. (**F**) Diagram of assay to test penetration of nanoparticles into an activated endothelial monolayer barrier and infiltration into non–P-selectin–expressing tumor spheroids, LX33, composed of primary human small cell lung cancer (SCLC) cells. (**G**) Targeted (FiPAX) and control (DexPAX) nanoparticle emission in the upper and lower chambers of a Transwell system. Plots show means ± SD ($n = 4$).

Author Manuscript
Author Manuscript
Author Manuscript
Author Manuscript

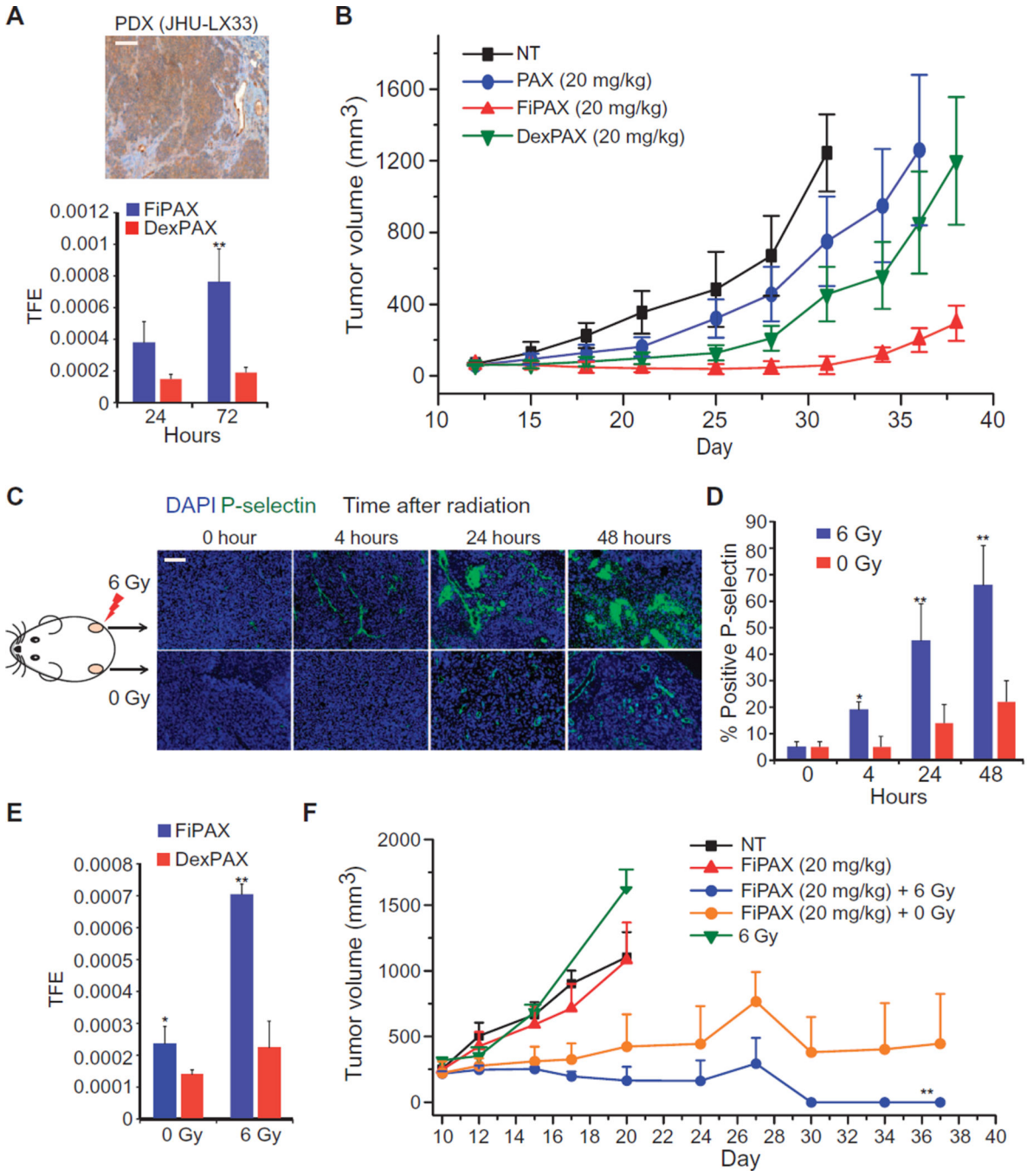

Fig. 3. Nanoparticle treatment of P-selectin–expressing and nonexpressing tumors in vivo

(**A**) Top: Tissue section of SCLC PDX stained with an antibody against P-selectin. Scale bar, 50 μm. Bottom: Targeted (FiPAX) and control (DexPAX) nanoparticle fluorescence in the PDX tumors, imaged in vivo 24 and 72 hours after injection. Bars show means ± SD of total fluorescence intensity from tumor region of interest (ROI); $n = 4$ per group; $P = 0.0091$. TFE, total fluorescence efficiency. (**B**) Tumor growth inhibition of PDX model after administration of a single dose of indicated treatments on day 12. Plot shows means ± SD ($n = 10$ per group). (**C**) Immunofluorescence measurements of 3LL tumors extracted from mice

Author Manuscript Author Manuscript Author Manuscript Author Manuscript

after radiation treatment. Green, P-selectin; blue, DAPI nuclear stain. Scale bar, 50 μm. (**D**) Percentage of blood vessels stained positive for P-selectin in the irradiated tissue at 4, 24, and 48 hours (respective *P* values are 0.058, 0.0041, and 0.0076). Blood vessels were stained with a CD31 antibody. (**E**) Targeted (FiPAX) and control (DexPAX) nanoparticle fluorescence from the right (irradiated) flank of 3LL-inoculated mice. Plot shows means ± SD; $n = 5$; $P = 0.0096$. (**F**) Tumor growth inhibition after irradiation and single-dose administration of drug treatments. All treatments were given on day 10 after tumor inoculation. The color key lists nanoparticle concentrations in terms of the amount of encapsulated drug. FiPAX (20 mg/kg) + 6 Gy refers to the tumors on the irradiated (right) flanks of the mice, and (FiPAX, 20 mg/kg) + 0 Gy refers to the tumors on the unirradiated (left) flanks of the same irradiated mice. The other groups refer to the tumors on separate animals receiving no treatment (NT), nanoparticles only (FiPAX, 20 mg/kg), or radiation only (6 Gy). $P = 0.0016$; $n = 5$ mice per group. Plots show means ± SD.

Author Manuscript Author Manuscript Author Manuscript Author Manuscript

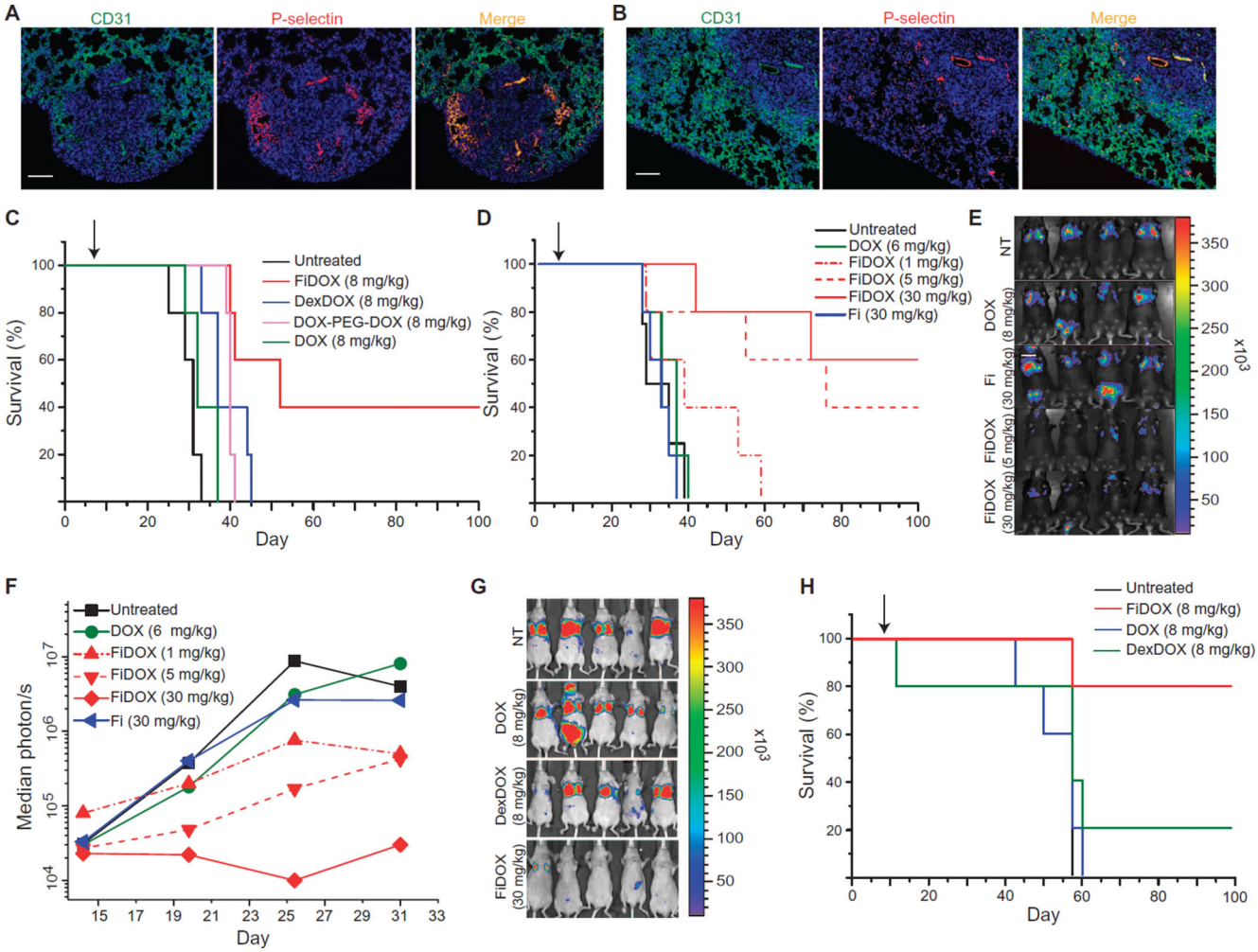

Fig. 4. P-selectin–targeted nanoparticle treatment of metastatic cancer models

(**A**) Representative images of P-selectin and vasculature (CD31) staining in a B16F10 melanoma experimental lung metastasis model 14 days after inoculation. Scale bar, 50 μm. (**B**) Representative images of P-selectin and CD31 staining in an MDA-MB-231 breast cancer experimental lung metastasis model 18 days after inoculation. Scale bar, 50 μm. (**C** and **D**) Survival data from two experiments using the B16F10 model treated 7 days after tumor inoculation with a single intravenous administration of the indicated treatments. (**E**) In vivo luciferase bioluminescence of the B16F10 model acquired 7 days after a single administration of the indicated treatments. (**F**) Median bioluminescence photon count from experiment shown in (D). (**G**) In vivo bioluminescence images acquired 21 days after a single administration of the indicated treatments to the luciferase-expressing MDA-MB-231 lung metastasis model. (**H**) Survival data from the MDA-MB-231 model treated on day 7 after inoculation with a single intravenous injection of the indicated treatments. The color key in each figure lists concentrations of nanoparticles and drug-polymer conjugates in terms of the amount of drug. Arrows denote day of administration for all treatments. $n = 5$ per group for all survival experiments.

Author Manuscript
Author Manuscript
Author Manuscript
Author Manuscript

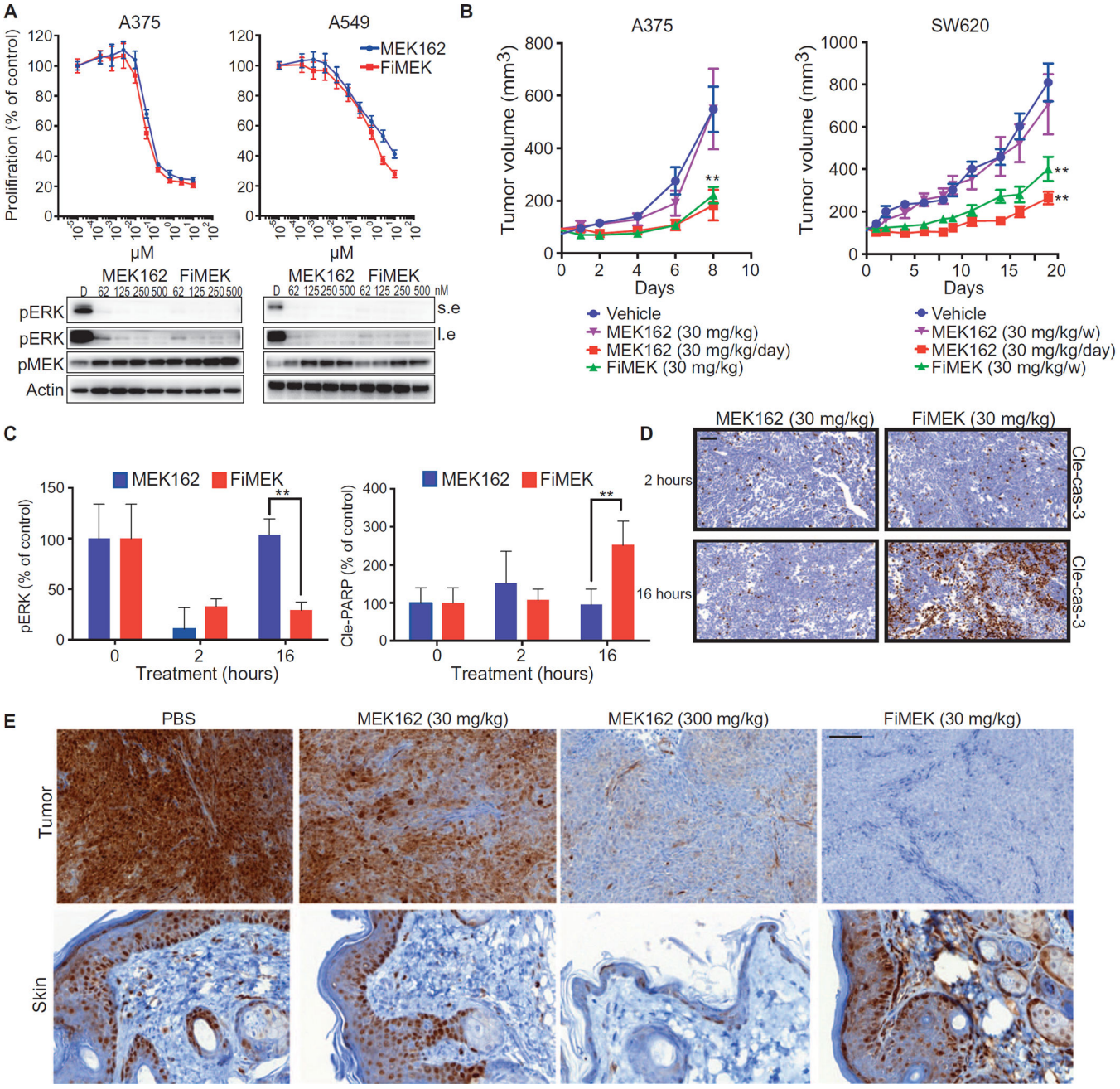

Fig. 5. P-selectin–targeted delivery of an inhibitor of the MEK/ERK pathway

(**A**) Top: Proliferation of cell lines measured after 4 days of treatment with MEK162 or FiMEK as indicated. Bottom: Biochemical analysis of A375 and A549 cell lines treated for 4 hours with MEK162 or FiMEK. (**B**) Growth of tumor xenografts after a single dose of vehicle, MEK162, and FiMEK or a daily dose of MEK162. *x* axis represents days after first treatment; $n = 6$ per group. $P^{(A375)} = 0.0048$, $P^{(SW520,FiMEK)} = 0.0071$, $P^{(SW520,MEK)} = 0.0055$. (**C**) Biochemical quantification (Western blot) of pERK and PARP cleavage in xenografts of A375 tumors treated for 2 or 16 hours with MEK162 or FiMEK. $P = 0.0089$ and 0.0053, respectively. (**D**) IHC of cleaved caspase 3 in HCT116 xenografts treated with

Author Manuscript Author Manuscript Author Manuscript Author Manuscript

MEK162 or FiMEK. Scale bar, 50 μm. (**E**) IHC of pERK in skin and tumors of HCT116 xenografts treated with MEK162 (30 and 300 mg/kg) or FiMEK (30 mg/kg) after 24 hours. Scale bar, 100 μm. Nanoparticle concentrations are listed in terms of the equivalent amount of encapsulated drug. Plots show means ± SD.